ACS OMEGA

Open Access

http://pubs.acs.org/journal/acsodf

Article

Unveiling the Three-Step Model for the Interaction of Imidazolium-Based Ionic Liquids on Albumin

Juliana Raw, Leandro R. Franco, Luiz Fernando de C. Rodrigues, and Leandro R. S. Barbosa*

Cite This: *ACS Omega* 2023, 8, 38101−38110

Read Online

ACCESS | Metrics & More | Article Recommendations | Supporting Information

ABSTRACT: The effect of the ionic liquids (ILs) 1-methyl-3-tetradecylimidazolium chloride ([C_{14}MIM][Cl]), 1-dodecyl-3-methylimidazolium chloride ([C_{12}MIM][Cl]), and 1-decyl-methylimidazolium chloride ([C_{10}MIM][Cl]) on the structure of bovine serum albumin (BSA) was investigated by fluorescence spectroscopy, ultraviolet−visible (UV−vis) spectroscopy, small-angle X-ray scattering (SAXS), and molecular dynamics (MD) simulations. Concerning the fluorescence measurements, we observed a blue shift and a fluorescence quenching as the IL concentration increased in the solution. Such behavior was observed for all three studied imidazolium-based ILs, being larger as the number of methylene groups in the alkyl chain increased. UV−vis absorbance measurements indicate that even at relatively small IL/protein ratios, like 1:1 or 1:2, ([C_{14}MIM][Cl]) is able to change, at least partially, the sample turbidity. SAXS results agree with the spectroscopic techniques and suggest that the proteins underwent partial unfolding, evidenced by an increase in the radius of gyration (R_g) of the scattering particle. In the absence and presence of ([C_{14}MIM][Cl]) = 3 mM BSA R_g increases from 29.1 to 45.1 Å, respectively. Together, these results indicate that the interaction of BSA with ILs is divided into three stages: the first stage is characterized by the protein in its native form. It takes place for protein/IL ≤ 1:2, and the interaction is predominantly due to the electrostatic forces provided by the negative charges on the surface of BSA and the cationic polar head of the ILs. In the second stage, higher IL concentrations induce the unfolding of the protein, most likely inducing the unfolding of domains I and III, in such a way that the protein's secondary structure is kept almost unaltered. In the last stage, IL micelles start to form, and therefore, the interaction with protein reaches a saturation point and free micelles may be formed. We believe that this work provides new information about the interaction of ILs with BSA.

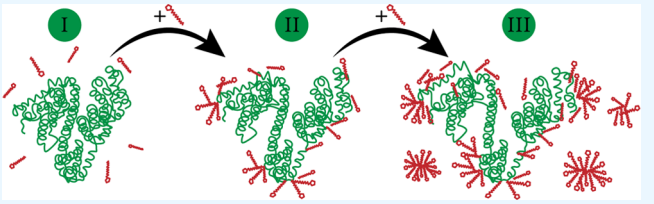

INTRODUCTION

The development of sustainable procedures and the use of molecules that are less harmful to the environment have been encouraged by the awareness of the industry and regulatory agencies. Organic solvents are one of the main environmental impact factors in chemical processes; therefore, greener substitutes are increasingly in demand. Ionic liquids (ILs) are the result of these efforts, and, in particular, surfactant ionic liquids have shown great success in this area.[1] ILs are salts that are liquid at temperatures smaller than 100 °C. ILs have interesting physicochemical properties like negligible vapor pressure, low degree of flammability, and high ionic conductivity.[2,3] The small vapor pressure ensures the ionic liquids its "green chemistry" use.[4] Since ILs can be exploited as an alternative solvent to the traditional organic ones (like chloroform or hexane), they can be used to improve electronic components[5,6] and also in biocatalysis processes.[7,8]

Protein−surfactant interactions are an important field of study due to their applications in personal care, pharmaceuticals, cosmetics, detergents, and bioscience.[9,10] Surfactants can denature,[11] unfold,[12] and refold proteins,[9,10,13] according to the properties, structure, and concentration of the protein and the surfactant being studied.[14] The nature of both molecules also determines the predominant interaction between the three main forces of this system: electrostatic, hydrophobic, and van der Waals.[15] Despite a large amount of research on the interaction of ILs and surfactants with biologically relevant systems, a systematic study of the imidazolium-based IL on model proteins, such as bovine serum albumin (BSA), is still indispensable.

Serum albumin proteins are essential to life: they are considered transport proteins and are the most abundant protein in the blood at a concentration of ≈42 mg/mL,[16] with such high concentration being crucial to its stability.[17] Bovine serum albumin (BSA) has been used as a model protein for many biophysical and biochemical studies as a model protein, in particular for ultraviolet−visible (UV−vis) spectroscopy, steady-state fluorescence, and small-angle X-ray scattering (SAXS), due to their water solubility and flexible binding capacity and capability to be used at different pHs,[17] urea

Received: June 13, 2023
Accepted: September 8, 2023
Published: October 5, 2023

concentrations,[18] and temperatures. BSA is made up of around 585 amino acid residues with a molecular weight of ≈66 kDa and is negatively charged at physiological pH (since its pI is around 5.4[17]). From the spectroscopic point of view, BSA has two tryptophan residues (TRP134 and TRP212), and when folded, TRP134 is located on the surface, more exposed to the solvent, whereas TRP212 is buried inside, less accessible. The interaction of model proteins with cationic amphiphilic molecules was already investigated in the literature: for instance, Chakraborty et al.[19] studied the interaction of BSA with cationic surfactants like dodecyltrimethylammonium bromide (DTAB), tetradecyltrimethylammonium bromide (TTAB), and cationic hexadecyltrimethylammonium bromide (CTAB), nonionic $C_{12}E_8$ surfactants, and anionic sulfate dodecyl sodium (SDS) surfactants. The authors reported that the BSA−SDS interaction is bimodal, while the BSA−cationic surfactant interaction increases with increasing tail length and is monomodal; according to the authors, cationic surfactants denatured BSA in a single step. ILs are expected to contribute in applications for drug delivery systems, but a better understanding of the mechanisms of action is needed.[20,21] This work provides new knowledge of the interaction between the imidazolium-based IL and proteins. In light of this new information, the application of ionic liquids in systems of biological interest or the development of new ionic liquids may be more specific and accurate.

Herein, we studied the interaction of three alkyl-functionalized imidazolium-based ILs with BSA, in order to get more information about the effects of ILs on different BSA structural levels. To do so, we used a combination of steady-state fluorescence, circular dichroism, small-angle X-ray scattering techniques, and molecular dynamics simulations.

MATERIALS AND METHODS

Materials. Bovine serum albumin with stated purities higher than 99% was purchased from Sigma-Aldrich, Germany. 1-Methyl-3-tetradecylimidazolium chloride ([C_{14}MIM][Cl]), 1-dodecyl-3-methylimidazolium chloride ([C_{12}MIM][Cl]), and 1,3-didecyl-2-methylimidazolium chloride ([C_{10}MIM]-[Cl]) with purity >98% are purchased from io-li-tec (Salzstrasse, Germany). All solutions were prepared in 20 mM acetate borate phosphate buffer (pH 7.3). Such buffer was chosen because we do know BSA behavior at pHs from 2.0−9.0.[17] BSA solutions were freshly prepared, and all measurements were performed at 22 ± 1 °C. Stock solutions of ILs at 200 mM were prepared in the same buffer. After this, samples were produced at the desired molar ratio between BSA and the ionic liquids.

Methods. *Steady-State Fluorescence.* Fluorescence measurements were performed using a Cary Eclipse-Vian spectrometer and a quartz cuvette of 2 mm optical path length. The fluorescence emission spectra were collected from 305 to 500 nm using an excitation wavelength of 295 nm (i.e., using tryptophan as an intrinsic probe) and slit width for excitation of 5 nm and for emission of 5 nm. We chose 295 nm as the excitation wavelength to minimize the excitation of phenylalanine and tyrosine residues. All spectra shown in this work were corrected by inner filter effects using the following equation[22,23]

$$F_{corr} = F_{obs} 10^{(A_{ex}+A_{em})/2} \quad (1)$$

where F_{corr} is the corrected fluorescence intensity, F_{obs} is the experimentally measured intensity, A_{ex} is the absorbance at the excitation wavelength (295 nm), and A_{em} is the absorbance at the emission.

A quantitative analysis of suppression is possible using the Stern−Volmer model fit. Some equations are used for the Stern−Volmer adjustment. We used the equation with the most satisfactory results, compatible with those obtained through other experimental techniques:[24,25]

$$\frac{F_0 - F}{F_0 - F_c} = \frac{[P]_t + [L]_t + K_d - \sqrt{([P]_t + [L]_t + K_d)^2 - 4[P]_t[L]_t}}{2[P]_t} \quad (2)$$

where $[P]_t$ is the protein concentration, F_0 is the protein fluorescence integral in the absence of ligand, F is the fluorescence integral in the presence of ligand, $[L]_t$ is the ligand concentration, and F_c is the integral of the remaining fluorescence. K_d is the fit parameter and dissociation constant. The inverse of the dissociation constant is defined as the binding constant, $K_a = 1/K_d$.

Circular Dichroism. CD measurements were performed with a JASCO-815 CD spectropolarimeter within the wavelength range of 195−260 nm. For recording the CD spectrum, a scan speed of 100 nm/min and a spectral bandwidth of 2.00 nm were maintained as parameters. A quartz cuvette with a 1 mm path length was used for the entire study. The following equation was used to convert the Theta machine units (θ, millidegrees) in mean residue ellipticity (MRE, degrees·cm^2·dmol^{-1}·residue^{-1})

$$\text{MRE} = \frac{\theta\ (\text{mdeg})}{C_p \times n \times l \times 10} \quad (3)$$

where C_p = molar concentration of the protein, n = number of amino acid residues, and l = cell path length. The α-helical content was calculated using the following equation adjusted for the BSA protein[26]

$$\alpha\text{-helix}\ (\%) = \frac{-\text{MRE}_{208} - 4000}{33000 - 4000} \times 100 \quad (4)$$

where MRE_{208} is the mean residue ellipticity at 208 nm.

Small-Angle X-ray Scattering. SAXS measurements were performed on the SAXS1 beamline of LNLS, using a Pilatus 300 K detector positioned at ∼1000 mm from the sample. All measurements were performed by using a sample holder with a path length of 1 mm and made of two mica windows. All SAXS measurements were performed at 22 ± 1 °C. The SAXS intensity of an isotropic solution of monodisperse particles is given by

$$I(q) = kP(q)S(q) \quad (5)$$

where k is a factor related to the instrumental effects and to the particle number density, q is the scattering vector, $P(q)$ is the particle form factor, and $S(q)$ is the structure factor. $S(q) \sim 1$ for diluted (not interacting) systems, so $I(q)$ is proportional to $P(q)$. In the current work, we use the Guinier approximation to calculate the radius of gyration (R_g) as follows

$$I(q \to 0) = I(0)e^{-R_g^2 q^2/3} \quad (6)$$

https://doi.org/10.1021/acsomega.3c04188
ACS Omega 2023, 8, 38101−38110

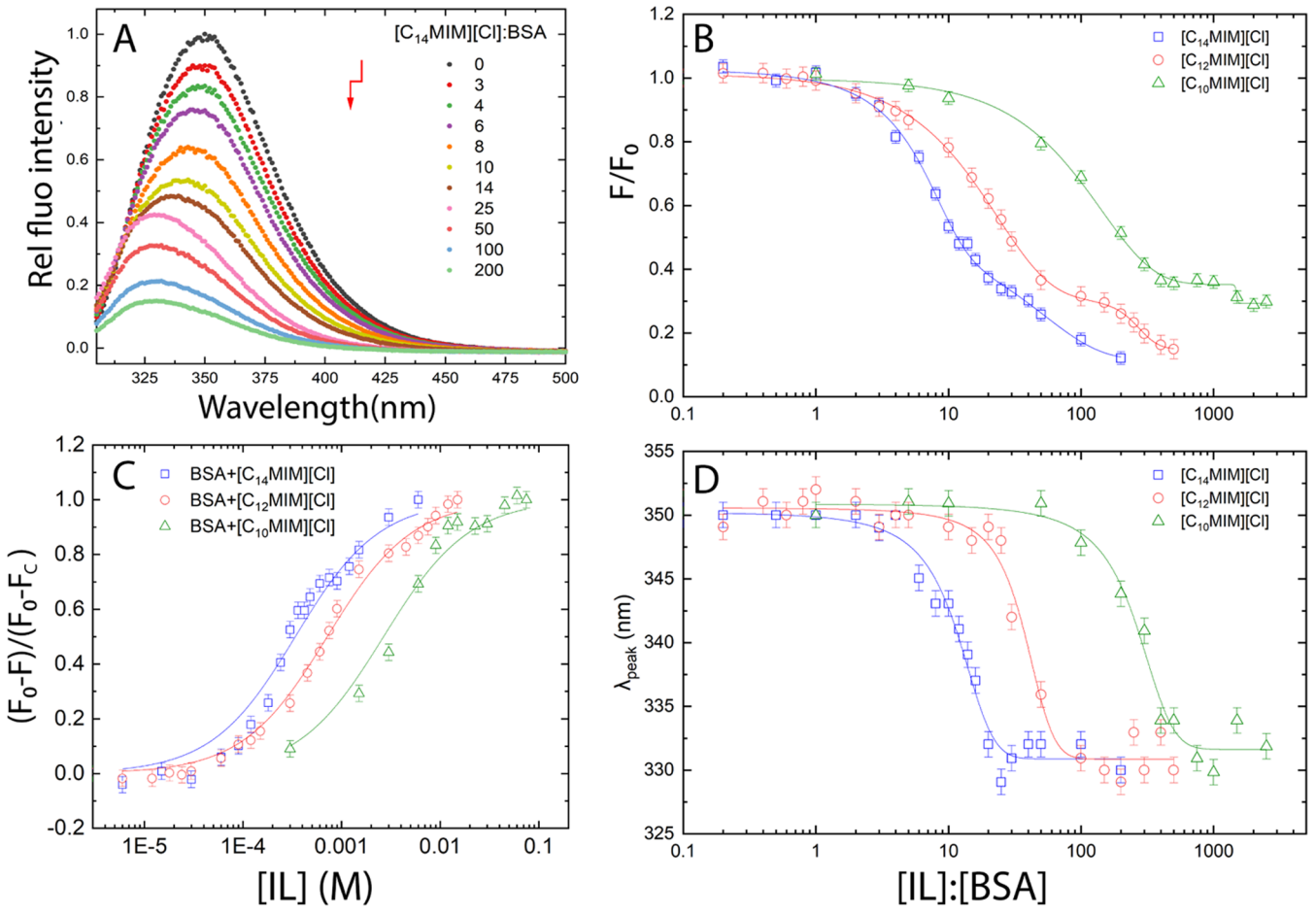

Figure 1. (A) Relative fluorescence emission spectra of 30 μM BSA (λ_{ex} = 295 nm) in the absence and presence of the gradual addition of [C_{14}MIM][Cl]. Molar ratios [IL]/[BSA] are in the legend (IL concentration increases along the arrow). (B) Ratio between the total fluorescence intensity (the integral under each fluorescence spectra) in the absence and presence of an increasing IL concentration as a function of molar ratio [IL]/[BSA] on a linear-log scale. (C) Stern−Volmer plot as a function of IL concentration on a linear-log scale. (D) The wavelength at the maximum emission of fluorescence as a function of molar ratio [IL]/[BSA] on a linear-log scale.

Noteworthily, Guinier's law can only be applied in the $q_{max}R_g \leq 1.3$ range (for approximately globular proteins) and for noninteracting systems.[27]

Molecular Dynamics simulations. We have performed molecular dynamics (MD) simulations of BSA in aqueous 1-methyl-3-tetradecylimidazolium chloride ([C_{14}MIM][Cl]) solutions in 4 different concentrations: 1 BSA and 0 [C_{14}MIM][Cl] (control simulation), 1 BSA and 10 [C_{14}MIM][Cl], 1 BSA and 100 [C_{14}MIM][Cl], and 1 BSA and 200 [C_{14}MIM][Cl]. The simulated systems were composed of 1 BSA, 16 sodium counterions to neutralize the protein charge, and N water molecules in a very large cubic box with a side length around 16 nm (N = 117,000 for 1 BSA/0 [C_{14}MIM][Cl], N = 116,697 for 1 BSA/10 [C_{14}MIM][Cl], N = 115,623 for 1 BSA/100 [C_{14}MIM][Cl], N = 114,243 for 1 BSA/200). The simulations were run in an NPT ensemble at 1 atm pressure and 298.15 K temperature. The velocity rescaling thermostat[28] was used to regulate temperature with a coupling constant of 0.1 ps, and the Berendsen barostat[29] was used to control pressure with a coupling constant of 2 ps to create the NPT ensemble. All interactions were calculated within a 14-cutoff radius. With cubic interpolation, a 14-bit Fourier spacing, and the smooth particle-mesh Ewald approach, an extended correction for electrostatic interactions was taken into account. The leapfrog algorithm was used to integrate the equations of motion.[30] The LINC[31] method was used with a time step of 2 fs and constraints in all H bonds. At each system level, the center of mass motion was linearly removed. The simulations were previously thermalized for 10 ns, and the production phase consisted of 300 ns for the simulations containing 0 or 10 [C_{14}MIM][Cl] and 500 ns for the simulations containing 100 or 200 [C_{14}MIM][Cl]. The Gromos54A7[32,33] force field was adopted for BSA and [C_{14}MIM][Cl], and the SPC/E[34] model was adopted for water. The simulations were performed in the Gromacs 5.1.4 package.[35]

RESULTS

Fluorescence Quenching and Shift of BSA by ILs. The fluorescence spectra of BSA at 30 μM in the absence and presence of increasing IL concentrations are shown in Figure 1A. Figure 1A shows that the fluorescence of BSA gradually decreases (quenching) and shifts (blue shift) with [C_{14}MIM][Cl] addition. This behavior is similar to others reported in the literature with ionic and nonionic surfactants.[36,37] Fluorescence quenching requires proximity between the fluorophore and its quencher,[38] so we can suggest that there is an interaction between the ILs and BSA, at least with one of the tryptophans present in the protein at positions TRP134 and TRP212. The systems containing the ionic liquids [C_{12}MIM][Cl] and [C_{10}MIM][Cl] exhibited a similar behavior as [C_{14}MIM][Cl]

https://doi.org/10.1021/acsomega.3c04188
ACS Omega 2023, 8, 38101−38110

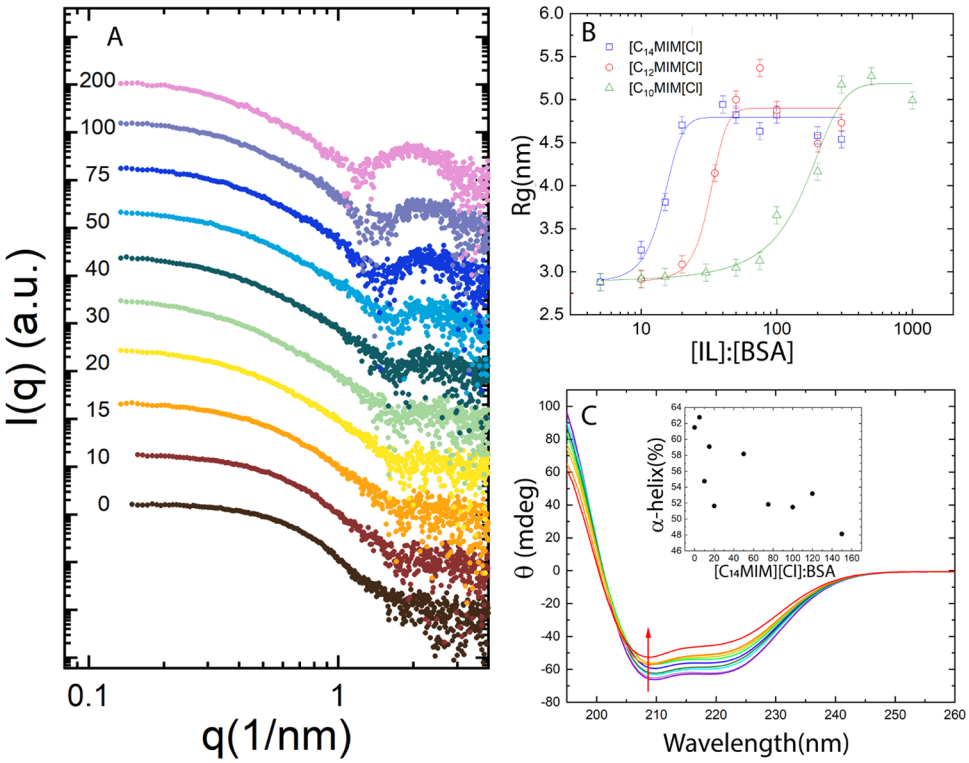

Figure 2. (A) SAXS data of 60 μM BSA in the absence and presence of the gradual addition of [C_{14}MIM][Cl]. Molar ratios [IL]/[BSA] are on the left. Curves are displaced vertically for clarity. (B) Radii of gyration in the absence and presence of an increasing IL concentration as a function of molar ratio [IL]/[BSA] on a linear-log scale. The solid curve is used to guide the eyes. (C) Circular dichroism spectra of BSA in the absence and presence of the gradual addition of [C_{14}MIM][Cl]. Insert graph shows %α-helix content as a function of the molar ratio [C_{14}MIM][Cl]. The IL concentration increases along the arrow.

system, with the only discernible distinction being the concentration of ionic liquid needed to induce the same effect, as illustrated in Figure S1.

The ratio between the total fluorescence intensity in the presence of the IL and that in the absence of the IL (F/F_0) is shown in Figure 1B. F/F_0 was calculated by dividing the integral of the fluorescence spectrum in the presence of an ionic liquid by the integral of the fluorescence spectrum in the absence of an ionic liquid. Stern−Volmer plot for the quenching of fluorescence intensity using eq 2 is shown in Figure 1C. Figure 1D shows the wavelength of the maximum emission of fluorescence as a function of IL concentration.

Concerning the quenching effect, from Figure 1B, we observed that total fluorescence intensity decreased by 50% at the molar ratios of 12 ± 1, 30 ± 3, and 202 ± 3 of [C_{14}MIM][Cl]/BSA, [C_{12}MIM][Cl]/BSA, and [C_{10}MIM]-[Cl]/BSA, respectively. This result indicates that the length of the alkyl chain plays a relevant role in the IL/BSA interaction; in other words, the longer the alkyl chain, the stronger the binding. In addition, that effect could be related to the hydrophobic characteristic of such interaction. The Stern−Volmner plot was adjusted according to eq 2 to obtain K_a values, Figure 1C.

Interestingly, K_a is larger as the carbon chain length increases as follows: (30 ± 2) × 10^2 M^{-1}, (14.3 ± 0.7) × 10^2 M^{-1}, and (3.8 ± 0.4). 10^2 M^{-1} in the presence of [C_{14}MIM][Cl], [C_{12}MIM][Cl], and [C_{10}MIM][Cl], respectively. The K_a values were calculated in order to compare the interaction of BSA with the 3 ILs; however, for a more reliable obtainment of the binding constant, other techniques are more adequate, such as isothermal titration calorimetry. Nevertheless, this result reinforces the importance of the hydrophobic component in the IL/water interaction.

Figure 1D can be divided into 3 different regions, as follows. In the first region, there is a plateau around 350.5 ± 0.5 nm that extends, in a molar ratio (i.e., [IL]/[BSA]), from 0:1 to 2:1, from 0:1 to 8:1, and from 0:1 to 50:1 of [C_{14}MIM][Cl]/BSA, [C_{12}MIM][Cl]/BSA, and [C_{10}MIM][Cl]/BSA, respectively. In this first stage, at small IL concentrations, there is no significant change in the emission peak wavelength. In the second region, however, there is a significant decrease in wavelength (i.e., a blue shift), starting from 350.5 ± 0.5 nm and reaching the minimum value of 331 ± 1 nm for all ionic liquids (at the reported concentrations), which was quite unexpected (Figure 1D). This second stage shows a blue shift in lower IL concentrations with higher alkyl chain lengths. In the third region, a new plateau was observed around 331 ± 1 nm, starting at molar ratios of 35:1, 100:1, and 1000:1 for [C_{14}MIM][Cl], [C_{12}MIM][Cl], and [C_{10}MIM][Cl], respectively. This third stage evidences a saturation-like behavior in the interaction of the protein and the amphiphilic molecules.

The fluorescence results we found are in agreement with other studies reported in the literature on the interaction of albumins with surfactants or ionic liquid surfactants. The interaction of the nonionic surfactant Hecameg with BSA shows the same behavior in three stages.[36] The first stage is ascribed to an initial noncooperative binding process, the second to a cooperative binding, and the third to a saturation binding region.

The gradual blue shift with increasing IL concentrations may indicate a more hydrophobic environment near tryptophan.[38] However, Vivian and Callis[39] demonstrated that the proximity

https://doi.org/10.1021/acsomega.3c04188
ACS Omega 2023, 8, 38101−38110

of charges or dipoles can alter tryptophan emission for both shorter and longer wavelengths, depending on the orientation. Therefore, a deeper discussion will be conducted along with the results of molecular dynamics.

Influence of ILs on the Protein Tertiary Structure. In order to get structural information on the IL/protein interaction, we performed SAXS measurements on 60 μM BSA in the absence and presence of an increasing IL concentration. The respective scattering curves are presented in Figure 2A. The curves are vertically shifted to emphasize the different scattering profiles, mainly in the high q range.

Figure 2A shows the formation of a peak at q = 0.23 Å^{-1} as the molar ratio [C_{14}MIM][Cl]/BSA increases. Such a peak is a fingerprint of the micellar form factor from SAXS measurements. Then, the data were analyzed through R_g using the Guinier approximation and are shown in Figure 2B.

Figure 2B reveals the R_g increase from (29 ± 1)Å in the absence of ILs to (46 ± 1)Å in the presence of 2.4 mM of [C_{14}MIM][Cl], and after such a concentration, a plateau is reached. In the absence of ILs, the R_g value is in good agreement with the reported 30 Å for the native crystallographic structure.[40] This demonstrates that BSA is unfolding with IL interaction, saturating at 2.4 mM [C_{14}mim][Cl]. This value is higher than the critical micellar concentration of this IL in buffer (1.0 ± 0.1 mM calculated with superficial tension—data not shown); therefore, further binding of the IL on the protein does not occur, and there is the coexistence of micelles and BSA−IL complex. The SAXS data, as illustrated in Figure S2, displayed similar trends across all three systems; however, in the [C_{10}MIM][Cl] system, the formation of micelle-like structures could not be observed. This discrepancy may be attributed to the possibility that the required concentration of [C_{10}MIM][Cl] for the formation of these structures was not reached.

ILs Are Able to Slightly Decrease the α-Helix Content of BSA. CD is an important tool for investigating modifications in proteins' secondary structure. BSA is a protein that has mostly α-helix structures in its native state, which is reflected in two negative minima in the CD spectrum at 208 and 222 nm wavelengths.[41] The literature report values between 60 and 67% of α-helix for native BSA.[42] The %α-helix is maximum when the BSA is in its native state and decreases in its unfolded state.[43]

The CD spectrum is shown in Figure 2C. It is possible to observe that, in general, the minimum value at 222 nm increases as [C_{14}MIM][Cl] concentration increases (see red arrow on Figure 2C), so there is an indication that the ionic liquid modifies the secondary structure even slightly. The inset in Figure 2C shows the α-helix of BSA calculated by using eqs 3 and 4. BSA in its native state, in the absence of ILs, presents 61.5% of the α-helix, which is in good accordance with the literature. Note that there is a downward trend in the α-helical content, reaching 48.1% at 150 molar ratios. Such values indicate that the protein is unfolding. [C_{12}MIM][Cl] and [C_{10}MIM][Cl] have a similar but smoother behavior. The lowest α-helix found with [C_{12}MIM][Cl] and [C_{10}MIM][Cl] are 52.3 and 54.6% at 300 and 50 molar ratios, respectively (data not shown).

Chakraborty et al.[19] studied physicochemical and conformational changes in BSA-surfactant systems using different biophysical approaches, like circular dichroism, viscosimetry, turbidity, and isothermal titration calorimetry (ITC), and surface tension measurements. They reported two interesting physical constants, namely, c_0, and c_1. The first one is the surfactant concentration where the system turbidity begins to increase, i.e., the system somehow is starting to change (surely, these are quite small numbers) due to the surfactant−protein interaction. The second one, on the other hand, is related to the surfactant concentration, where the surface tension reaches a plateau, i.e., all of the added surfactants beyond this point are probably making micelles in the bulk solution, and this should be understood as a saturation point. Interestingly, they reported a value of 67% of α-helix content for BSA in the absence of surfactants, in good accordance with the literature.[18] On the other hand, they reported values of α-helix for BSA as 46, 46, and 49% in the presence of the cationic hexadecyltrimethylammonium bromide (CTAB), tetradecyltrimethylammonium bromide (TTAB), and dodecyltrimethylammonium bromide (DTAB), respectively, at surfactant concentrations smaller than c_0, i.e., at small cationic surfactant concentrations. Nevertheless, the authors also report values for α-helix for BSA of 12, 16, and 15%, for CTAB, TTAB, and DTAB, respectively, beyond c_1, i.e., at surfactant saturation conditions. Such a fact indicates that at higher concentrations these cationic surfactants can really unfold BSA, up to a certain point. Therefore, in terms of the denaturing potential of BSA, ionic liquids are comparable to CTAB, TTAB, and DTAB (cationic surfactants) before c_0, i.e., at a small ionic liquid concentration. Unfortunately, we were not able to measure larger IL concentrations using CD due to the chemical nature of our IL, which absorbs UV light.

Investigating the Location of ILs on a BSA Surface Using Molecular Dynamic Simulations. To shed some light on the IL effects on the BSA structure and electronic properties, we have performed MD simulations of BSA in aqueous solution and at 3 different concentrations of [C_{14}MIM][Cl] ionic liquids (1 BSA/10 IL, 1 BSA/100 IL, and 1 BSA/200 IL). The root-mean-square deviation (RMSD) of BSA, for the backbone or all atoms, did not show significant changes in the free IL simulation or in those ones at the 1/10 and 1/100 BSA/IL concentrations (Figure S3). But, at the highest IL concentration, 1 BSA/200 IL, it has increased around 5% between 200 and 300 ns of simulation, equilibrating after that. Such structural changes are mainly related to the protein radius of gyration enhancement (Figure 3), from 2.67 ± 0.17 nm in free IL simulation to 2.89 ± 0.03 nm in 1 BSA/200 IL simulation, that probably occurs in the region of residues 550−583, as revealed by the root-mean-square fluctuation (RMSF) analysis (Figure S4). Although the calculated changes in the BSA radius of gyration are smaller than the experimental observations and in the absence and presence of [C_{14}MIM][Cl] at 3 mM, it has increased from 2.9 to 4.5 nm, respectively, the theoretical tendency is in agreement with our experimental findings, demonstrating that at high ionic liquid concentrations, the interaction between BSA and the IL can indeed cause an increase of the protein radius of gyration.

The solvation shells around BSA are quite different in the simulations at high (100 or 200 IL per BSA) and lower ionic liquid concentrations (0 or 10 IL per BSA). At the highest concentrations, the cationic [C_{14}MIM][Cl] molecule causes strong dehydration of the protein, where lots of water/BSA hydrogen bonds are broken (Figure 4B) and a considerable area around the protein is occupied by the cationic [C_{14}MIM][Cl] molecules. After equilibration, the number of BSA/water hydrogen bonds is approximately 1192 ± 23, 1160

https://doi.org/10.1021/acsomega.3c04188
ACS Omega 2023, 8, 38101−38110

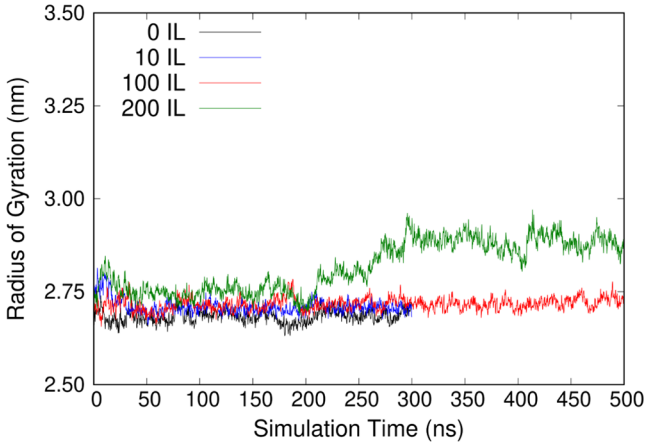

Figure 3. Radius of gyration of BSA in pure water (in black) and in IL/water solutions at different concentrations (1 BSA/10 IL in blue, 1 BSA/100 IL in red, and 1 BSA/200 IL in green). All simulations were performed using $[C_{14}MIM][Cl]$ ionic liquid since it was the one with a larger effect on the protein structure according to our experimental data.

$\pm$ 23, 985 $\pm$ 24, and 960 $\pm$ 21 for the systems with 0, 10, 100, and 200 IL, respectively. It means that at the highest IL concentration, around 250 BSA/water hydrogen bonds have disappeared during the simulation. The solvent distribution around the protein can also be mapped by the radial distribution functions between BSA and the ionic liquid and water molecules (Figure S5). The integral of such functions shows that the number of $[C_{14}MIM][Cl]$ molecules surrounding the protein increases according to the concentration of the IL in the solution. For example, up to a distance of 2 nm between the centers of mass of the protein residues and the $[C_{14}MIM][Cl]$ molecules, it is found out a total of 9, 7, and 1 $[C_{14}MIM][Cl]$ molecules surrounding the protein at the concentrations 1 BSA/10 IL, 1 BSA/100 IL, and 1 BSA/200 IL, respectively. These numbers increase to 26, 19, and 3 for a distance of 3 nm and to 70, 53, and 8 for a distance of 5 nm, respectively. Figure 4C,D shows MD snapshots of the $[C_{14}MIM][Cl]$ distribution around BSA for the 1 BSA/200 IL simulation at 50 and 500 ns. Those $[C_{14}MIM][Cl]$ molecules which are not found close to the protein solvent accessible area form small aggregates containing up to 12 $[C_{14}MIM][Cl]$ units.

On the other hand, the IL did not affect the secondary structure of BSA. The coil, bend, turn, α-helix, and 3-helix percentages were quite similar in any simulation (Figure S6). The calculated percentages of the α-helix were 67, 69, 68, and 69% in the systems with 0, 10, 100, and 200 IL, respectively. These numbers are close to our experimental prediction that

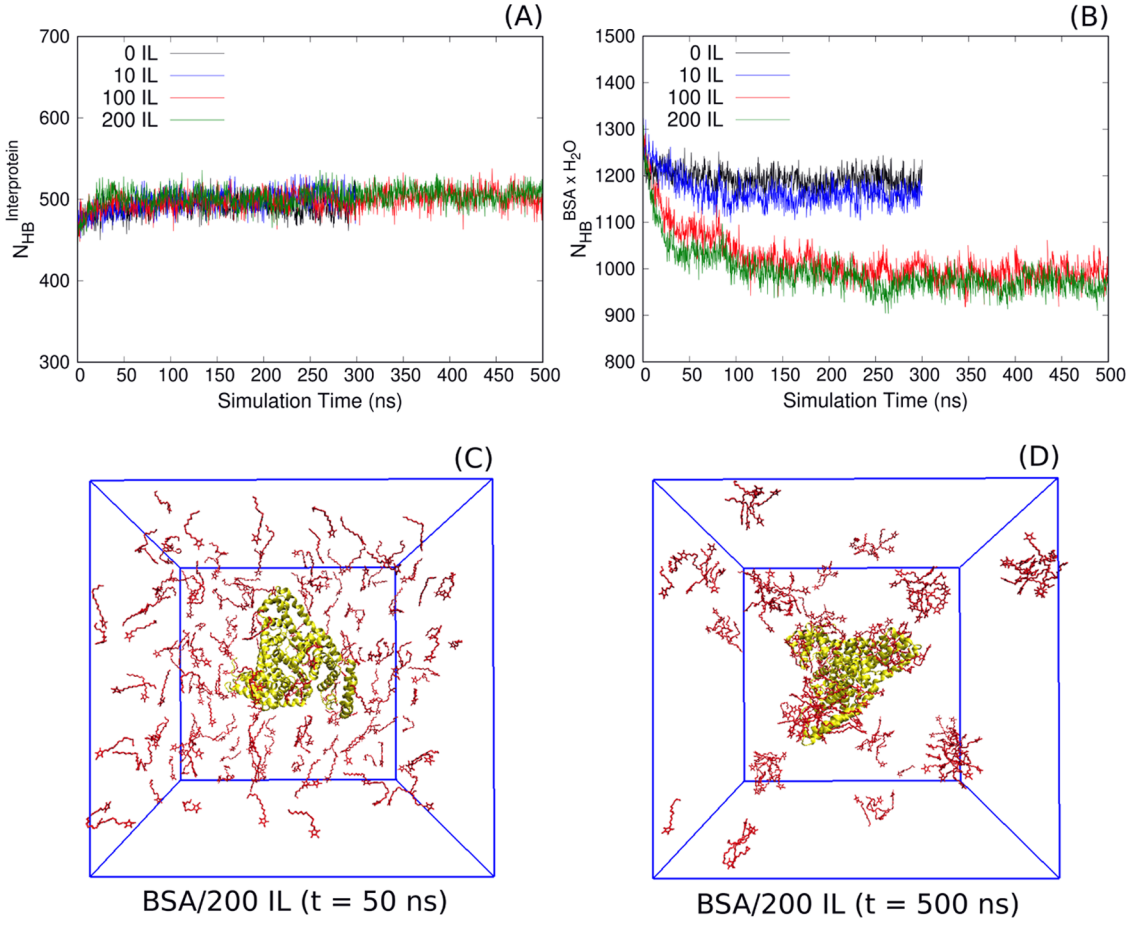

Figure 4. (A) Number of intramolecular and (B) intermolecular hydrogen bonds for simulations of BSA in pure water (in black) and in ionic liquid (IL)/water solutions in different concentrations (1 BSA/10 IL in blue, 1 BSA/100 IL in red, and 1 BSA/200 IL in green). (C, D) Snapshots extracted from the simulation of BSA/200 IL showing the protein (in yellow) and the $C_{14}MIM$ molecules (in red), for simulation times t = 50 ns (C) and t = 500 ns (D); water molecules and counterions were excluded in the images for better visualization.

https://doi.org/10.1021/acsomega.3c04188
ACS Omega 2023, 8, 38101−38110

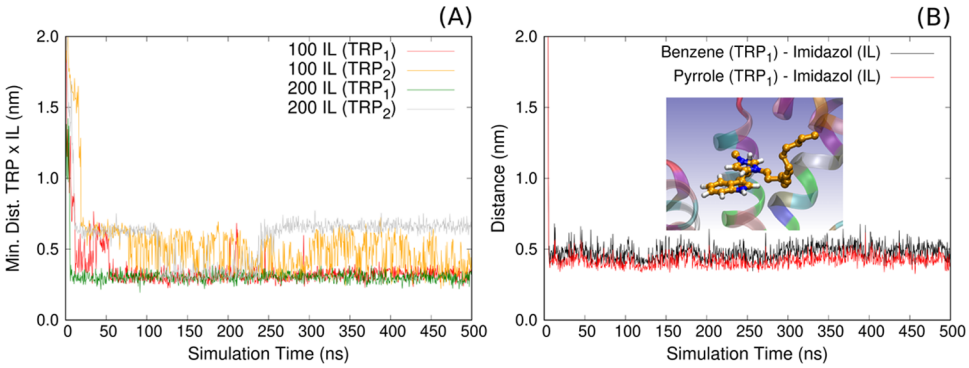

Figure 5. (A) Minimum distance between the tryptophan residues (TRP1 and TRP2) and the C14 IL molecules for BSA in ionic liquid/water solutions of different concentrations (1 BSA/100 and 1 BSA/200 IL). (B) Center of mass distances between the benzene and pyrrole rings of TRP1 and the imidazole ring of C14 for BSA in ionic liquid/water solution at 1 BSA/200 IL concentration.

was 66% and agree with the theoretical observation that the number of BSA intermolecular hydrogen bonds does not change during simulations as well (Figure 4A), being 501 ± 13, 503 ± 11, 504 ± 11, and 505 ± 11 in the systems with 0, 10, 100, and 200 IL, respectively. Moreover, based on our analysis, in the simulations with high IL concentrations (1 BSA/100 IL or 1 BSA/200 IL), approximately 30% of all $[C_{14}MIM][Cl]$ molecules are observed to be bound to the protein within a maximum distance of 0.5 nm, while the remaining 70% of $[C_{14}MIM][Cl]$ molecules form small aggregates consisting of up to 12 units. In the simulation at a lower IL concentration (1 BSA/10 IL), all $[C_{14}MIM][Cl]$ molecules are bound to the protein.

Finally, we analyzed the $[C_{14}MIM][Cl]$ distribution around the two Trp residues. Quite interestingly, in the simulations with 100 or 200 IL, a single $[C_{14}MIM][Cl]$ molecule was found close to the most exposed Trp of BSA (TRP1, the TRP134) interacting with it in a type of $\pi-\pi$ stacking configuration, with the imidazole ring of $[C_{14}MIM][Cl]$ parallel to the TRP1 pyrrole and benzene rings, with a binding energy of −6.5 ± 2.0 kcal/mol. Such a configuration was observed before the first 10 ns (or 60 ns) of simulation for the system with 200 IL (or 100 IL) and remained during the entire simulation without $[C_{14}MIM][Cl]$ exchanges. The same was not observed for the buried Trp (TRP2, or TRP212), which was found reasonably close only to the extremity of any $[C_{14}MIM][Cl]$ tail that has entered the protein structure. Figure 5A shows the minimum distance between the tryptophan residues (TRP1 and TRP2) and $[C_{14}MIM][Cl]$ molecules over the simulations. For the last 200 ns of simulation, the TRP1−$[C_{14}MIM][Cl]$ minimum distance is on average 0.30 ± 0.10 nm (or 0.34 ± 0.10 nm) for the 1 BSA/200 IL (or 1 BSA/100 IL) system and the TRP2−$[C_{14}MIM][Cl]$ minimum distance is on average 0.58 ± 0.22 nm (or 0.52 ± 0.26 nm) for the 1 BSA/200 IL (or 1 BSA/100 IL) system.

The TRP1/$[C_{14}MIM][Cl]$ $\pi-\pi$ stacking interaction was a surprising result. Analyzing the MD configurations, we observed that the center of mass distance from the pyrrole TRP1 ring to the imidazole $[C_{14}MIM][Cl]$ ring (0.41 ± 0.2 nm) is approximately 0.9 Å smaller than the distance from the benzene TRP1 ring to the imidazole $[C_{14}MIM][Cl]$ ring (0.50 ± 0.2 nm, see Figure 5B). In other words, the positive +1 charge of the $C_{14}MIM$ imidazole is closer to that of the pyrrole ring than to that of the benzene ring of TRP1. This is an important observation that has an impact on the spectroscopy properties of BSA in ionic liquid solution. Vivian and Callis[39] reported theoretical results where they have predicted the fluorescence wavelengths of 19 tryptophans in 16 proteins and demonstrated that a positive charge over the tryptophan pyrrole ring induces a blue shift on the emission spectra of the protein. Therefore, our MD simulation findings can explain the measured blue shift in the emission spectra of BSA at high IL concentrations.

We can suppose that the IL, at least in high concentrations, induces a structural change in BSA, increasing its radius of gyration. The regions within the BSA structure that most contribute to such modifications can be identified from the RMSF as a function of the position of the BSA residue, as shown in Figure S4.

Through RMSF analysis of the BSA structure, we can notice that there are more flexible and dynamic regions within the structure than others, even in the absence of ILs. We highlight the 110−120 region for BSA in the presence of 100 molecules of ILs and the 500−535 and 560−583 regions for BSA in the presence of 200 molecules of ILs.

In the RMSF plot, we can observe that the main peaks are in the α-helices of subdomain III. Subdomain III, in addition to possessing important binding sites, is also the subdomain that undergoes the most modifications during the protein denaturation process due to changes in pH.[44,45]

DISCUSSION

These results suggest that the interaction of BSA with the ILs can be divided into three stages, as shown in Figure 6. The first stage is characterized by native protein, when electrostatic forces were predominating, provided by the opposing charges on the surface of the proteins and the polar head of the ILs. The approximation of the IL to the surface of the protein allows the interaction between the hydrophobic sites of the protein with the carbon chains of the ILs. The hydrophobic effect is a relevant contributor to the interaction in the second stage, potentiating the formation of the protein−IL complex. In the last stage, the interaction between the protein and the IL decreases. The formation of IL micelles in solution starts and occurs at the binding saturation of ILs to proteins.

The results of fluorescence spectroscopy obtained for BSA in the presence of $[C_{14}MIM][Cl]$, $[C_{12}MIM][Cl]$, and $[C_{10}MIM][Cl]$ show an interaction between the protein and the IL, more specifically near the tryptophan, inducing a quenching and a blue shift. Analysis of the radius of gyration from SAXS curves shows BSA unfolding with IL interaction.

https://doi.org/10.1021/acsomega.3c04188
ACS Omega 2023, 8, 38101−38110

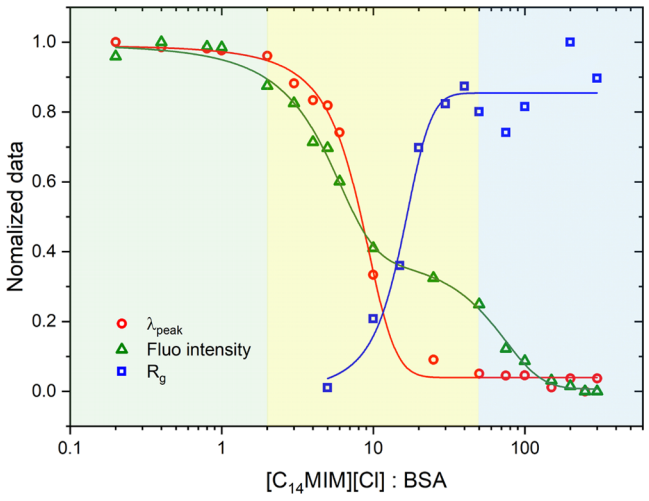

Figure 6. Normalized data from 0 to 1 of the fluorescence shift, quenching, and radius of gyration.

These results indicate that the interaction of BSA with the IL is divided into three stages, as explained earlier (Figure 6).

In their study, Singh and Kang[46] looked at how the BSA protein self-assembled in aqueous solutions of functionalized and unfunctionalized ionic liquids. Depending on the structure and concentration of the ILs, the effects on the self-assembled BSA generated by $[C_{12}MIM][Cl]$, $[C_{12}AMIM][Cl]$, and $[C_{12}EMIM][Cl]$ are all different. The authors saw large, chaotic self-assembled BSA structures, ordered self-assembled structures like lengthy rods, and right-handed twisted helical amyloid fibers. The results obtained by these authors align with our findings regarding $[C_{12}MIM][Cl]$, including quenching, a blue-shift in fluorescence emission, indications of protein unfolding, and the coexistence of protein/IL complexes and micelle-like IL structures. We propose to further interpret the blue-shift phenomenon as a consequence of the positive charge of the ionic liquid in proximity to the pyrrole TRP134 ring and the dehydration of the protein, as revealed by molecular dynamics data. These interactions provide valuable insights into the observed spectral shifts. Moreover, Scanavachi et al.,[47] studied the influence of partially unfolded bovine serum albumin (BSA) in the absence and presence of hydrogenated and fluorinated surfactants (SDS and SPFO, respectively). The authors utilized molecular dynamics simulations and experimental biophysical tools to better understand the protein aggregation process, induced by both surfactants. Interestingly, the differences in the chemical structure of the surfactants, particularly the presence of fluorine atoms in SPFO, impose distinct steric restrictions on the binding to the unfolded protein, inducing different aggregate shapes and internal organization. The partially unfolded BSA induced by low pH obtained by MDS is similar to what we are proposing the the present study.

It is well-known that disulfide bonds are chemically stable in the absence of a reduction agent, which is our case since the bond cannot be reduced by the ionic liquid. Another way to avoid a disulfite bond is to perform a mutation in the Cys residue, which was not performed in the present study. Thus, from our perspective and under the experimental conditions used herein, it is straightforward to conclude that all 17 disulfide bonds remain unaltered during the ionic liquid/protein interaction. Such a fact can justify the secondary structure of BSA even at higher IL concentrations.

According to the data presented herein, it is possible to propose a mechanism of action for the studied imidazolium ionic liquids with BSA. On this ground, Figure 7 shows a schematic representation of the primary and secondary structure of BSA. Such a figure was assembled on the PDB website using the 4F5S entry for the protein. Figure 7 shows in the first line the protein residue number (ranging from 1−583), as well as the regions with α-helix structures (the red rectangles in the second line of the figure) and, most interestingly, the connection between each cysteine pair for the 34 BSA cysteine residues. Moreover, in the last line, we have the position of domain I (from residue 1−185), domain II (from residue 186−378), and domain III (from residue 379−583). The data presented herein support the model that the unfolding process starts with the increase in the distance between domains I and III, in such a way that the protein keeps its secondary structure. Moreover, it should be stressed that there are no cysteine bonds between domains. BSA has a heart-shaped structure, thus domains I and III are almost in contact. The significance of this research relies on its potential applications in the pharmaceutical industry, where the use of ionic liquids as solvents, stabilizers, and drug delivery systems is gaining importance. Understanding the interactions between serum albumin and ionic liquids can provide valuable information for the development of more effective drug formulations and delivery systems with improved bioavailability and enhanced therapeutic outcomes.

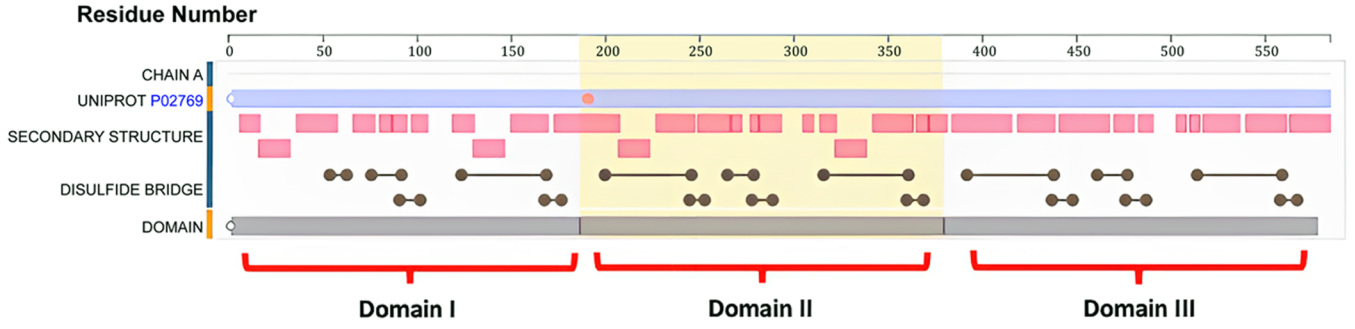

Figure 7. Schematic representation of bovine serum albumin primary and secondary structure, indicating the main structural features, like domain I (from residue 1−185), domain II (from residue 186−378), and domain III (from residue 379−583). It is also indicated in the figure the regions with α-helix structures (red rectangular boxes) and all 17 disulfide bonds, involving the 34 cysteines (round circles connected with solid lines). These data represent the PDB entry 4F5S. This figure was created at uriwww.pdb.org.

https://doi.org/10.1021/acsomega.3c04188
ACS Omega 2023, 8, 38101−38110

■ ASSOCIATED CONTENT

Supporting Information

The support information file has: The Supporting Information is available free of charge at https://pubs.acs.org/doi/10.1021/acsomega.3c04188.

Relative fluorescence emission spectra and the SAXS curves of BSA in the absence and presence of gradual addition of $[C_{14}MIM][Cl]$, $[C_{12}MIM][Cl]$, and $[C_{10}MIM][Cl]$; figures about the root-mean-square deviation (RMSD) and root-mean-square fluctuations (RMSF) of the BSA backbone in pure water and in the presence of ionic liquids at different concentrations; radial distribution function; $g(r)$ of BSA and water; and secondary structure of BSA (PDF)

■ AUTHOR INFORMATION

Corresponding Author

Leandro R. S. Barbosa − *Department of General Physics, University of São Paulo, Institute of Physics, São Paulo 05508-000 SP, Brazil; Brazilian Synchrotron Light Laboratory (LNLS), Brazilian Center for Research in Energy and Materials (CNPEM), Campinas 13083-100 SP, Brazil;* orcid.org/0000-0001-5997-2160; Phone: +55 1935121044; Email: lbarbosa@if.usp.br

Authors

Juliana Raw − *Department of General Physics, University of São Paulo, Institute of Physics, São Paulo 05508-000 SP, Brazil*

Leandro R. Franco − *Department of Engineering and Physics, Karlstad University, Karlstad 65188, Sweden;* orcid.org/0000-0002-8692-3396

Luiz Fernando de C. Rodrigues − *Department of General Physics, University of São Paulo, Institute of Physics, São Paulo 05508-000 SP, Brazil; Brazilian Synchrotron Light Laboratory (LNLS), Brazilian Center for Research in Energy and Materials (CNPEM), Campinas 13083-100 SP, Brazil*

Complete contact information is available at: https://pubs.acs.org/10.1021/acsomega.3c04188

Notes

The authors declare no competing financial interest.

■ ACKNOWLEDGMENTS

This work was supported by FAPESP (2015/15822-1, 2016/05019-0, 2017/26131-5) and CNPq. L.R.S.B. has research fellowships from CNPq (309418/2021-6). The authors thank the National Council for Scientific and Technological Development (CNPq) and Coordination for the Improvement of Higher Education (CAPES) for a research fellowship. This research used facilities of the Brazilian Synchrotron Light Laboratory (LNLS, for SAXS measurements, proposal #20180204), and the Bioenewables National Laboratory (LNBR, for CD measurements, proposal LAM-20102) both are part of the Brazilian Center for Research in Energy and Materials (CNPEM), a private nonprofit organization under the supervision of the Brazilian Ministry of Science, Technology, and Innovations (MCTI). The SAXS1 beamline staff members are acknowledged for their assistance during the experiments. The Biophysics of Macromolecules (BFM) staff is also acknowledged for the assistance during the experiments. We conducted the computational modeling using the High-Performance Computing (HPC) Cluster provided by the University of São Paulo.

■ REFERENCES

(1) Buettner, C. S.; Cognigni, A.; Schröder, C.; Bica-Schröder, K. Surface-active ionic liquids: A review. *J. Mol. Liq.* **2022**, *347*, No. 118160.

(2) Welton, T. Room-temperature ionic liquids. Solvents for synthesis and catalysis. *Chem. Rev.* **1999**, *99*, 2071−2084.

(3) Mu, T.; Han, B. *Structures and Interactions of Ionic Liquids*; Zhang, S.; Wang, J.; Lu, X.; Zhou, Q., Eds.; Springer Berlin Heidelberg: Berlin, Heidelberg, 2014; pp 107−139.

(4) Greaves, T. L.; Drummond, C. J. Protic Ionic Liquids: Properties and Applications. *Chem. Rev.* **2008**, *108*, 206−237.

(5) He, P.; Liu, H.; Li, Z.; Liu, Y.; Xu, X.; Li, J. Electrochemical Deposition of Silver in Room-Temperature Ionic Liquids and Its Surface-Enhanced Raman Scattering Effect. *Langmuir* **2004**, *20*, 10260−10267.

(6) Kim, T. Y.; Lee, H. W.; Stoller, M.; Dreyer, D. R.; Bielawski, C. W.; Ruoff, R. S.; Suh, K. S. High-performance supercapacitors based on poly(ionic liquid)-modified graphene electrodes. *ACS Nano* **2011**, *5*, 436−442.

(7) Attri, P.; Choi, E. H. Influence of Reactive Oxygen Species on the Enzyme Stability and Activity in the Presence of Ionic Liquids. *PLoS One* **2013**, *8*, No. e75096.

(8) Park, S.; Viklund, F.; Huit, K.; Kazlauskas, R. Ionic Liquids as Green Solvent - Progress and Prospects. *ACS Symp. Ser.* **2003**, *856*, 225−238, DOI: 10.1021/bk-2003-0856.fw001.

(9) Pedersen, J. N.; Lyngsø, J.; Zinn, T.; Otzen, D. E.; Pedersen, J. S. A complete picture of protein unfolding and refolding in surfactants. *Chem. Sci.* **2020**, *11*, 699−712.

(10) Otzen, D. E.; Pedersen, J. N.; Rasmussen, H. Ø.; Pedersen, J. S. How do surfactants unfold and refold proteins? *Adv. Colloid Interface Sci.* **2022**, *308*, No. 102754.

(11) Blanco, E.; Ruso, J. M.; Prieto, G.; Sarmiento, F. On relationships between surfactant type and globular proteins interactions in solution. *J. Colloid Interface Sci.* **2007**, *316*, 37−42.

(12) Gull, N.; Sen, P.; Khan, R. H.; Kabir-Ud-Din. Spectroscopic studies on the comparative interaction of cationic single-chain and gemini surfactants with human serum albumin. *J. Biochem.* **2008**, *145*, 67−77.

(13) Kaspersen, J. D.; Søndergaard, A.; Madsen, D. J.; Otzen, D. E.; Pedersen, J. S. Refolding of SDS-Unfolded Proteins by Nonionic Surfactants. *Biophys. J.* **2017**, *112*, 1609−1620.

(14) Otzen, D. Protein−surfactant interactions: A tale of many states. *Biochim. Biophys. Acta, Proteins Proteomics* **2011**, *1814*, 562−591.

(15) Mackie, A.; Wilde, P. The role of interactions in defining the structure of mixed protein−urfactant interfaces. *Adv. Colloid Interface Sci.* **2005**, *117*, 3−13. A Collection of Papers from the International Workshop on Bubble and Drop Interfaces, Genoa, Italy, 25−28 April, 2004

(16) Peters, T. *All About Albumin*; Academic Press: San Diego, 1995.

(17) Barbosa, L. R.; Ortore, M. G.; Spinozzi, F.; Mariani, P.; Bernstorff, S.; Itri, R. The importance of protein-protein interactions on the pH-induced conformational changes of bovine serum albumin: A small-angle x-ray scattering study. *Biophys. J.* **2010**, *98*, 147−157.

(18) Itri, R.; Caetano, W.; Barbosa, L. R. S.; Baptista, M. S. Effect of urea on bovine serum albumin in aqueous and reverse micelle environments investigated by small angle X-ray scattering, fluorescence and circular dichroism. *Braz. J. Phys.* **2004**, *34*, 58−63.

(19) Chakraborty, T.; Chakraborty, I.; Moulik, S. P.; Ghosh, S. Physicochemical and Conformational Studies on BSA Surfactant Interaction in Aqueous Medium. *Langmuir* **2009**, *25*, 3062−3074.

(20) Egorova, K. S.; Gordeev, E. G.; Ananikov, V. P. Biological Activity of Ionic Liquids and Their Application in Pharmaceutics and Medicine. *Chem. Rev.* **2017**, *117*, 7132−7189.

(21) Han, Q.; El Mohamad, M.; Brown, S.; Zhai, J.; Rosado, C.; Shen, Y.; Blanch, E. W.; Drummond, C. J.; Greaves, T. L. Small angle

X-ray scattering investigation of ionic liquid effect on the aggregation behavior of globular proteins. *J. Colloid Interface Sci.* **2023**, *648*, 376−388, DOI: 10.1016/j.jcis.2023.05.130.
(22) Sur, S. S.; Rabbani, L. D.; Libman, L.; Breslow, E. Fluorescence studies of native and modified neurophysins.Effects of peptides and pH+. *Biochemistry* **1979**, *18*, 1026−1036.
(23) Mendonça, A. F.; Rocha, A. F. C.; Duarte, A. C.; Santos, E. B. H. The inner filter effects and their correction in fluorescence spectra of salt marsh humic matter. *Anal. Chim. Acta* **2013**, *788*, 99−107.
(24) Bakar, K. A.; Feroz, S. R. A critical view on the analysis of fluorescence quenching data for determining ligand−protein binding affinity. *Spectrochim. Acta, Part A* **2019**, *223*, No. 117337.
(25) van de Weert, M.; Stella, L. Fluorescence quenching and ligand binding: A critical discussion of a popular methodology. *J. Mol. Struct.* **2011**, *998*, 144−150.
(26) Bhogale, A.; Patel, N.; Mariam, J.; Dongre, P.; Miotello, A.; Kothari, D. Comprehensive studies on the interaction of copper nanoparticles with bovine serum albumin using various spectroscopies. *Colloids Surf., B* **2014**, *113*, 276−284.
(27) Svergun, D. I.; Koch, M. H. Small-angle scattering studies of biological macromolecules in solution. *Rep. Prog. Phys.* **2003**, *66*, 1735−1782.
(28) Bussi, G.; Donadio, D.; Parrinello, M. Canonical sampling through velocity rescaling. *J. Chem. Phys.* **2007**, *126*, No. 014101.
(29) Berendsen, H. J. C.; Postma, J. P. M.; van Gunsteren, W. F.; DiNola, A.; Haak, J. R. Molecular dynamics with coupling to an external bath. *J. Chem. Phys.* **1984**, *81*, 3684−3690.
(30) Hockney, R. W.; Goel, S. P.; Eastwood, J. W. Quiet high-resolution computer models of a plasma. *J. Comput. Phys.* **1974**, *14*, 148−158.
(31) Hess, B.; Bekker, H.; Berendsen, H. J. C.; Fraaije, J. G. E. M. LINCS: a linear constraint solver for molecular simulations. *J. Comput. Chem.* **1997**, *18*, 1463−1472.
(32) Huang, W.; Lin, Z.; van Gunsteren, W. F. Validation of the GROMOS 54A7 force field with respect to β-peptide folding. *J. Chem. Theory Comput.* **2011**, *7*, 1237−1243.
(33) Schmid, N.; Eichenberger, A. P.; Choutko, A.; Riniker, S.; Winger, M.; Mark, A. E.; Van Gunsteren, W. F. Definition and testing of the GROMOS force-field versions 54A7 and 54B7. *Eur. Biophys. J.* **2011**, *40*, 843−856, DOI: 10.1007/s00249-011-0700-9.
(34) Berendsen, H. J. C.; Grigera, J. R.; Straatsma, T. P. The missing term in effective pair potentials. *J. Phys. Chem. A* **1987**, *91*, 6269−6271.
(35) Van Der Spoel, D.; Lindahl, E.; Hess, B.; Groenhof, G.; Mark, A. E.; Berendsen, H. J. C. GROMACS: fast, flexible, and free. *J. Comput. Chem.* **2005**, *26*, 1701−1718.
(36) Hierrezuelo, J.; Nieto-Ortega, B.; Ruiz, C. C. Assessing the interaction of Hecameg with Bovine Serum Albumin and its effect on protein conformation: A spectroscopic study. *J. Lumin.* **2014**, *147*, 15−22.
(37) Gelamo, E. L.; Silva, C. H. T. P.; Imasato, H.; Tabak, M. Interaction of bovine (BSA) and human (HSA) serum albumins with ionic surfactants: spectroscopy and modelling. *Biochim. Biophys. Acta, Protein Struct. Mol. Enzymol.* **2002**, *1594*, 84−99.
(38) Lakowicz, J. R. *Principles of Fluorescence Spectroscopy*; Springer: US, 2009.
(39) Vivian, J. T.; Callis, P. R. Mechanisms of Tryptophan Fluorescence Shifts in Proteins. *Biophys. J.* **2001**, *80*, 2093−2109.
(40) Santos, S. F. A.; Zanette, D.; Fischer, H.; Itri, R. A systematic study of bovine serum albumin (BSA) and sodium dodecyl sulfate (SDS) interactions by surface tension and small angle X-ray scattering. *J. Colloid Interface Sci.* **2003**, *262*, 400−408.
(41) Corbin, J.; Méthot, N.; Wang, H. H.; Baenziger, J. E.; Blanton, M. P. Secondary structure analysis of individual transmembrane segments of the nicotinic acetylcholine receptor by circular dichroism and Fourier transform infrared spectroscopy. *J. Biol. Chem.* **1998**, *273*, 771−777.
(42) Halder, S.; Aggrawal, R.; Aswal, V. K.; Ray, D.; Saha, S. K. Study of refolding of a denatured protein and microenvironment probed through FRET to a twisted intramolecular charge transfer fluorescent biosensor molecule. *J. Mol. Liq.* **2021**, *322*, No. 114532.
(43) Halder, S.; Aggrawal, R.; Jana, S.; Saha, S. K. Binding interactions of cationic gemini surfactants with gold nanoparticles-conjugated bovine serum albumin: A FRET/NSET, spectroscopic, and docking study. *J. Photochem. Photobiol., B* **2021**, *225*, No. 112351.
(44) El Kadi, N.; Taulier, N.; Le Huérou, J. Y.; Gindre, M.; Urbach, W.; Nwigwe, I.; Kahn, P. C.; Waks, M. Unfolding and refolding of bovine serum albumin at acid pH: ultrasound and structural studies. *Biophys. J.* **2006**, *91*, 3397−3404.
(45) Baler, K.; Martin, O. A.; Carignano, M. A.; Ameer, G. A.; Vila, J. A.; Szleifer, I. Electrostatic Unfolding and Interactions of Albumin Driven by pH Changes: A Molecular Dynamics Study. *J. Phys. Chem. B* **2014**, *118*, 921−930.
(46) Singh, G.; Kang, T. S. Ionic Liquid Surfactant Mediated Structural Transitions and Self-Assembly of Bovine Serum Albumin in Aqueous Media: Effect of Functionalization of Ionic Liquid Surfactants. *J. Phys. Chem. B* **2015**, *119*, 10573−10585.
(47) Scanavachi, G.; Espinosa, Y. R.; Yoneda, J. S.; Rial, R.; Ruso, J. M.; Itri, R. Aggregation features of partially unfolded bovine serum albumin modulated by hydrogenated and fluorinated surfactants: Molecular dynamics insights and experimental approaches. *Journal of Colloid and Interface Science* **2020**, *572*, 9−21.

https://doi.org/10.1021/acsomega.3c04188
ACS Omega 2023, 8, 38101−38110